Icarus 410 (2024) 115897

Contents lists available at ScienceDirect

Icarus

journal homepage: www.elsevier.com/locate/icarus

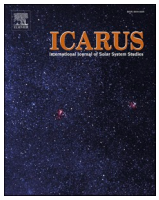

Is there H_2O stacking disordered ice I in the Solar System?

Christoph G. Salzmann [a,*], Benjamin J. Murray [b], Mark G. Fox-Powell [c], Rachael E. Hamp [c], Alexander Rosu-Finsen [a], Helen Fraser [c]

[a] Department of Chemistry, University College London, 20 Gordon Street, London WC1H 0AJ, UK
[b] Institute for Climate and Atmospheric Science, School of Earth and Environment, University of Leeds, Leeds LS2 9JT, UK
[c] AstrobiologyOU, The Open University, Milton Keynes MK7 6AA, UK

ARTICLE INFO

Keywords:
Ice phases
Physical properties (ices)
Solar system
Ice spectroscopy
Remote sensing

ABSTRACT

Water ice exists in large quantities across the Solar System, and it is involved in a wide range of atmospheric and geological processes. Here we focus on the question if stacking disordered ice I (ice I*sd*) is present in the Solar System. The conditions required to form ice I*sd* are described and we argue that previous descriptions of 'cubic ice' (ice I*c*) in the literature may in fact have been concerned with ice I*sd*. In contrast to the stable hexagonal ice I (ice I*h*) and ice I*c*, ice I*sd* is a highly complex material that encompasses a wide range of possible stacking regimes and structures. The most fundamental quantity to describe a given ice I*sd* sample is its cubicity which reflects the fraction of cubic stacking. Following an introduction into the characterisation techniques used to identify and characterise ice I*sd*, we discuss the various environments in the Solar System where ice I*sd* may exist and the relevance its existence may have. This includes the atmospheres of the inner planets, various icy moons as well as comets and other icy objects in the far reaches of the Solar System. The details of the stacking disorder may contain information about the formation and thermal history of ice I*sd* samples. This offers the exciting prospect of using ice I*sd* as a marker material for atmospheric and geological processes. The crystallographic space group of ice I*sd* allows polar structures which could be an important factor for the accretion of ice particles in space. We conclude that ice I*sd* should exist at several locations in the Solar System and in potentially large quantities. The definitive identification of ice I*sd* in a natural environment is a next major milestone in our understanding of the importance of water ice across the Solar System.

1. Introduction

Water (H_2O) is the third most abundant molecule in the Universe following dihydrogen (H_2) and carbon monoxide (CO) (Kwok, 2007). Travelling through the Solar System, water ice is a constant companion from the polar regions on Earth and the asteroid belt to the icy satellites of the gas giants and the Kuiper belt. The snow-line in the Solar System, beyond which volatiles such as water readily condense, is currently found between the asteroid belt and Jupiter (Jewitt et al., 2007). However, even closer to the Sun, ice can persist if it is not constantly exposed to sunlight such as in craters in the polar regions of Mercury (Deutsch et al., 2017) and the Moon (Li et al., 2018). The presence of ice across the Solar System is important for a variety of reasons: Firstly, ice can transform to liquid water which is the key component for the search for extra-terrestrial life. Secondly, the properties and phase transitions of the many different types of ice may influence atmospheric and geological processes. Finally, the presence of ice outside of Earth is an important technological factor for space exploration in terms of the creation of rocket fuel and water supply for crewed missions.

Despite the simplicity of the small *V*-shaped H_2O molecule, water displays remarkable structural complexity in its condensed forms including at present 20 crystalline forms (Millot et al., 2019; Prakapenka et al., 2021; Salzmann, 2019) and at least three families of amorphous ices (Burton and Oliver, 1935; Mishima et al., 1984; Rosu-Finsen et al., 2023). High-pressure phases of ice have been identified as diamond inclusions on Earth (Tschauner et al., 2018), they are thought to be major components of some of the icy moons in the Solar System (Hussmann et al., 2015; Journaux et al., 2020) and may exist as superionic forms in the interiors of the gas giants (Millot et al., 2019; Prakapenka et al., 2021).

At pressures below 0.2 GPa, ice I*h* is the stable form of ice sharing phase boundaries with the liquid and gas phase (Salzmann, 2019). This

* Corresponding author.
E-mail address: c.salzmann@ucl.ac.uk (C.G. Salzmann).

https://doi.org/10.1016/j.icarus.2023.115897
Received 1 October 2023; Received in revised form 22 November 2023; Accepted 25 November 2023
Available online 30 November 2023

is the phase of ice that we are all familiar with either in the form of ice cubes in our drinks, or snow and ice in nature. The crystal structure of ice I*h* consists of puckered layers of hydrogen-bonded water molecules forming six-membered rings. These layers are stacked on top of each other by always using the mirror image of the previous layer as indicated by the dashed line in Fig. 1(a). In addition to hexagonal stacking, the layers can also stack in a cubic fashion. Here, no mirror operation is used, instead the layers are shifted with respect to each other upon stacking as shown by the arrow in Fig. 1(b). Cubic ice I, or ice I*c*, contains only cubic stacking.

On the basis of diffraction data it was realised some time ago that so-called ice I*c* samples contained hexagonal stacking faults (Kuhs et al., 1987). Later, the diffraction data were modelled and analysed in a quantitative fashion, and it was found that complex combinations of hexagonal and cubic stacking are possible as shown, for example, in Fig. 1(c) (Hansen et al., 2008; Kuhs et al., 2012; Malkin et al., 2012; Malkin et al., 2015). The key quantity obtained from fitting the diffraction data is the cubicity, Φ_c, reflecting the fraction of cubic stacking of a given sample. The corresponding hexagonality, Φ_h, is then simply $1 - \Phi_c$. It was suggested that ice samples with Φ_c between 0.01 and 0.99 should be called stacking disordered ice (ice I*sd*) and that many of the previously described ice I*c* samples in the literature must in fact have been ice I*sd* (Malkin et al., 2015; Murray et al., 2015a). Pure ice I*c*, *i.e.* with $\Phi_c = 1$, was only discovered a few years ago which now makes the precise characterisation of the extent of stacking disorder in ice I even more pertinent (del Rosso et al., 2020; Komatsu et al., 2020; Salzmann and Murray, 2020).

Ice I*sd* and by extension ice I*c* are thermodynamically metastable with respect to ice I*h*. This means that they will transform to ice I*h* irreversibly if allowed by the kinetics of the exothermic phase transition. Their higher free energy implies a higher vapour pressure compared to ice I*h* (Nachbar et al., 2019; Rosu-Finsen et al., 2022; Shilling et al., 2006). The differences in crystal structure between the various members of the ice I family imply different crystal shapes, and hence light scattering properties (Murray et al., 2015b) as well as different spectroscopic properties (Carr et al., 2014; Celli et al., 2020).

Here, we first provide details about the formation, characterisation and phase transitions of ice I*sd*. We then discuss where ice I*sd* could be present in the Solar System, the consequences the presence of ice I*sd* may have on the various environments, how ice I*sd* may be detected in future space missions and how the details of the stacking disorder may be used as markers for the thermal history and parent materials of ice I*sd* samples. In contrast to the structurally well-defined ices I*h* and I*c*, ice I*sd* is a highly complex material encompassing a wide range of possible structures that will require state-of-the-art characterisation techniques in order to understand its potential importance across the Solar System.

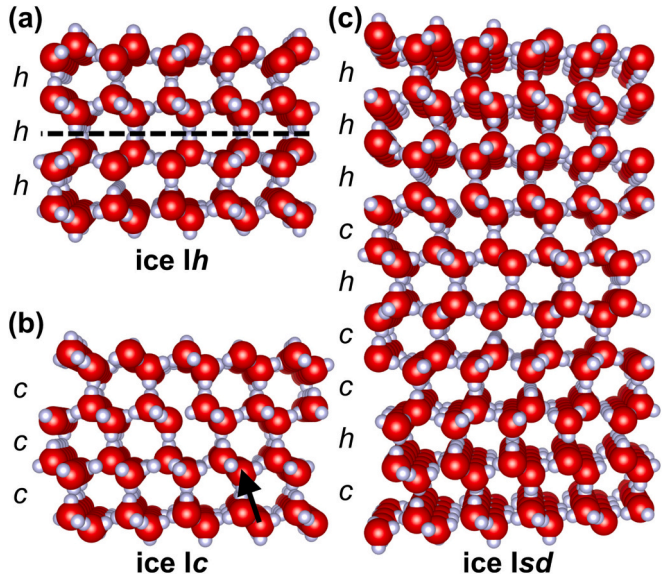

Fig. 1. Crystal structures of (a) hexagonal ice I*h*, (b) cubic ice I*c* and (c) a possible stacking sequence of stacking disordered ice I (ice I*sd*). Red and white spheres represent oxygen and hydrogen atoms, respectively. The structures show the orientational disorder of the hydrogen-bonded water molecules. The dashed line in (a) and the arrow in (b) indicate the mirror plane and the displacement vector associated with hexagonal (*h*) and cubic (*c*) stacking, respectively.

2. Formation, characterisation and phase transitions of ice I*sd*

2.1. Experimental pathways to ice I*sd*

The experimental procedures for making the different types of ice I are given in Table 1. Ice I*h* is obviously easy to make whenever the temperature is high enough so that thermodynamic equilibrium is quickly reached within the relevant pressure range. This can be achieved by cooling water vapour or liquid water at ambient pressure as well as through the decompression of ice III at temperatures close to the melting line. Ices I*sd* and I*c* are metastable, and transform to ice I*h* upon heating. Ice I*h* was also obtained at low temperatures in a phase mixture with ice IX upon heating high-density amorphous ice at 0.2 GPa. Despite the apparent ease of making ice I*h*, the preparation of large single crystals of ice I*h* without defects and gas inclusions is a major challenge (Petrenko and Whitworth, 1999).

A variety of experimental pathways to ice I*sd* exist. These include cooling water vapour or liquid water droplets quickly to low temperatures. Transforming liquid water to ice I*sd* can be aided by carrying out the freezing in confinement or by the addition of solutes. Heating low-density amorphous ice, the high-pressure phases of ice II, IV, V, VI, IX, XII and certain gas hydrates at ambient pressure also leads to the

Table 1
Experimental conditions for making the various types of ice I. All ambient-pressure procedures are expected to be valid under vacuum conditions.

Type of ice I	Experimental pathway of preparation	References
Ice I*h*	Slow freezing of liquid water or vapour deposition (frosting) at ambient pressure	(Hobbs, 1974)
Ice I*h*	Decompression of ice III	(Hobbs, 1974)
Ice I*h*	Ambient-pressure heating of ice I*sd* or ice I*c*.	(del Rosso et al., 2020; Komatsu et al., 2020; Kuhs et al., 2012; Rosu-Finsen et al., 2022)
Ice I*h*	Heating of high-density amorphous ice at 0.2 GPa	(Salzmann et al., 2004a)
Ice I*sd*	Low-temperature vapour deposition	(König, 1943)
Ice I*sd*	Hyperquenching of water droplets	(Kohl et al., 2000)
Ice I*sd*	Freezing of confined water	(Baker et al., 1997; Dowell et al., 1962; Malkin et al., 2012; Murray et al., 2005)
Ice I*sd*	Freezing of water containing solutes	(Elarby-Aouizerat et al., 1987; Kajiwara et al., 2008; Palacios et al., 2010; Vigier et al., 1987)
Ice I*sd*	Heating low-density amorphous ices at ambient pressure	(Dowell and Rinfret, 1960; McMillan and Los, 1965; Rosu-Finsen et al., 2023; Shephard et al., 2016)
Ice I*sd*	Heating high-pressure phases of ice at ambient pressure (ices II, IV, V, VI, IX, XII)	(Arnold et al., 1968; Bertie et al., 1963; Bertie et al., 1964; Kuhs et al., 1987; Salzmann et al., 2004b)
Ice I*sd*	Dissociation of gas clathrate hydrates upon heating at ambient pressure	(Falenty and Kuhs, 2009; Kuhs et al., 2004; Takeya et al., 2005)
Ice I*c*	Heating of ice XVII at ambient pressure	(del Rosso et al., 2020)
Ice I*c*	Decompression of hydrogen-filled high-pressure ice	(Komatsu et al., 2020)

formation of ice I*sd*. As discussed in more detail in the following, the nature of the parent phase has a substantial influence on the stacking characteristics of ice I*sd* (Hansen et al., 2008; Kuhs et al., 2012).

Ice I*c* can be obtained either by heating the empty C_0-structure clathrate hydrate ice XVII at ambient pressure (del Rosso et al., 2020) or decompression of a high-pressure hydrogen hydrate (Komatsu et al., 2020).

2.2. Structural characterisation of ice I*sd*

The most powerful technique for characterising the exact details of the stacking disorder in ice I*sd* is diffraction including powder X-ray and neutron diffraction. The crystallographic space groups of ices I*h*, I*sd* and I*c* are $P6_3/mmc$, $P3m1$ and $Fd\text{-}3m$ (Murray et al., 2015b). Fig. 2(a) shows how the X-ray diffraction patterns change as Φ_c increases upon going through various ice I*sd* states between ice I*h* to ice I*c*. The stacking disorder leads to broad and asymmetric diffraction features that affect some of the Bragg peaks. The corresponding neutron diffraction data for D_2O ice I is shown in Fig. S1.

The diffraction data in Fig. 2(a) and S1 were calculated using MCDIFFaX (Salzmann et al., 2015) assuming that the probabilities of cubic and hexagonal stacking are independent of the previous stacking event. In reality, stacking probabilities can depend on the previous stacking events resulting from so-called memory or Reichweite effects (Hart et al., 2018; Jagodzinski, 1949). The 'stackogram' plot in Fig. 2(b) shows the first-order stacking probabilities Φ_{cc} and Φ_{hc} which reflect the probabilities of cubic stacking following cubic or hexagonal stacking, respectively. Interestingly, all ice I*sd* samples characterised so far are located above the line of random stacking where $\Phi_{cc} = \Phi_{hc}$. This means that for ice I*sd* there is generally a tendency to stay within a giving stacking sequence rather than preferential switching between cubic and hexagonal stacking. So far, up to second-order memory effects have been included in the analysis of diffraction data of ice I*sd* (Hansen et al., 2008; Kuhs et al., 2012; Malkin et al., 2012; Malkin et al., 2015). Φ_c can be calculated from the higher order stacking probabilities (Salzmann et al., 2015) and lines of constant Φ_c are indicated in Fig. 2(b). It has been stressed that the correct analysis of the diffraction data of ice I*sd* requires the full modelling as performed, for example, by MCDIFFaX. Simple peak-intensity ratios of diffraction features do not correlate well with Φ_c (Hansen et al., 2014).

In addition to diffraction, the structure of ice I*sd* has been characterised with pair-distribution-function analysis (Playford et al., 2018). Consistent with the results from diffraction, the stacking disorder of ice I*sd* has recently been imaged with high-resolution electron microscopy (Huang et al., 2023). The Raman spectroscopic signature of stacking disorder in ice I has also been described (Carr et al., 2014). Increasing amounts of stacking disorder lead to a frequency increase by a few wavenumbers of the most intense feature of the O—H stretching band at around 3100 cm^{-1} and a decrease in intensity of this feature with respect to the other components of the spectroscopic band. Subtle differences in the lattice mode region around 250 cm^{-1} of the Raman spectra of ice I*c* and ice I*h* were recently pointed out (Celli et al., 2020).

2.3. Phase transitions of ice I*sd*

Fig. 2(c) shows how Φ_c of ice I*sd* obtained by crystallising vapour-

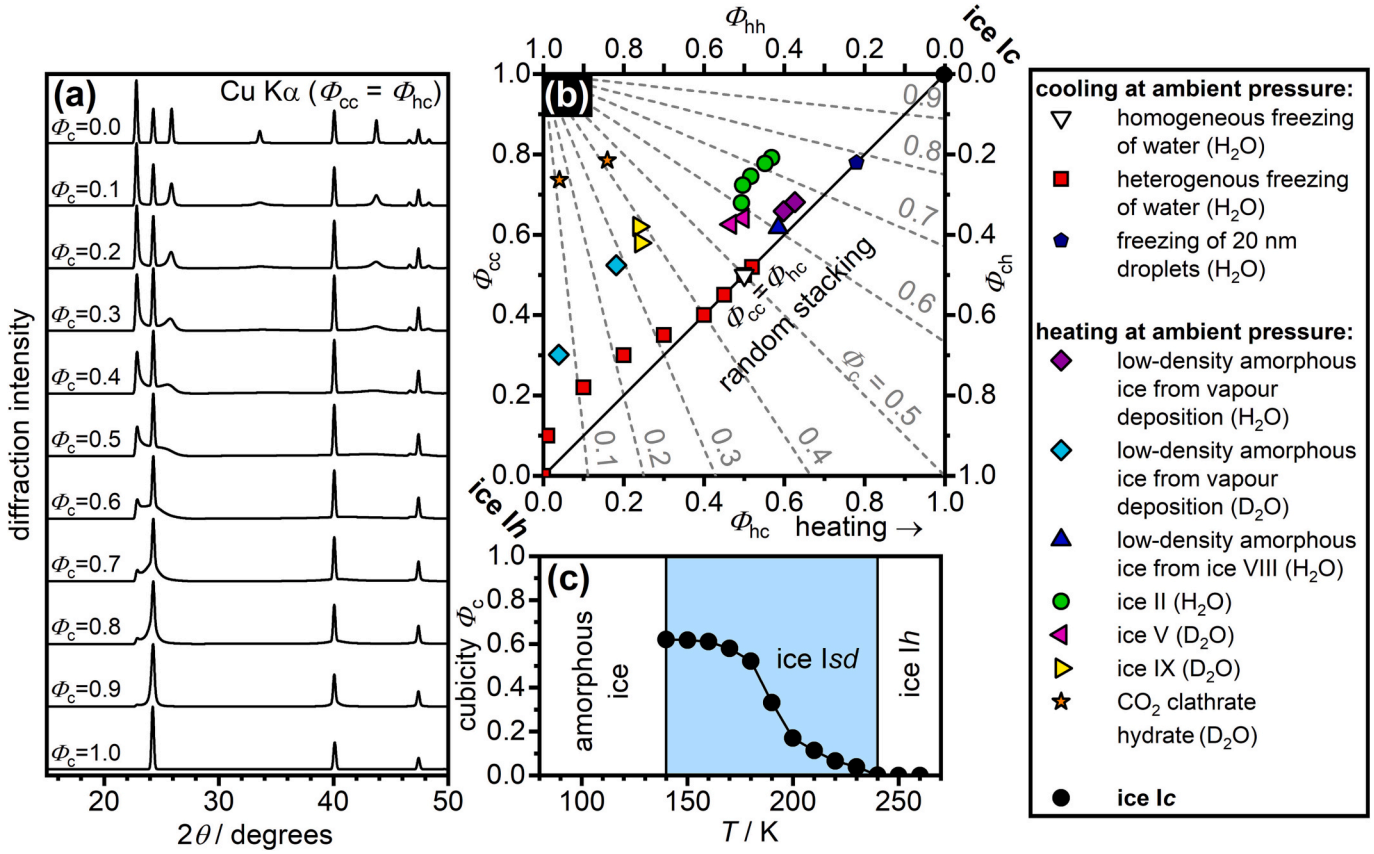

Fig. 2. (a) X-ray diffraction patterns (Cu Kα) calculated with MCDIFFaX for ice I structure with cubicities, Φ_c, from 0 to 1 and random stacking. (b) 'Stackogram' plot describing the structures of ice I*sd* by including first-order memory effects. The diagonal solid line indicates random stacking. Lines of constant Φ_c are shown as dashed grey lines. The formation procedures of the ice I*sd* samples are indicated in the legend with data taken from (Amaya et al., 2017; del Rosso et al., 2020; Halukeerthi et al., 2020; Komatsu et al., 2020; Kuhs et al., 2012; Malkin et al., 2012; Malkin et al., 2015; Shephard et al., 2016; Talewar et al., 2019). (c) Φ_c of H_2O ice I*sd* obtained by crystallising vapour-deposited amorphous ice (amorphous solid water) upon heating at ambient pressure (Rosu-Finsen et al., 2022).

deposited low-density amorphous ice (also known as amorphous solid water) changes upon heating. The Φ_c of the ice I*sd* after crystallisation is around 60% which illustrates clearly that this material should not be described as ice I*c*. The decrease in Φ_c upon heating is gradual starting at around 160 K and it reaches zero at around 240 K with the formation of fully hexagonal ice I*h* (Rosu-Finsen et al., 2022). As expected for the phase transition of a metastable material to the stable phase, the changes in Φ_c are irreversible. This means that cooling back at any point during the gradual change would not lead to an increase in Φ_c. Instead, the phase transition would slow down or even stop completely if the temperatures are low enough.

The phase transition from ice I*sd* to ice I*h* is weakly exothermic with transition enthalpies in the tens of J mol^{-1} (Handa et al., 1986; Handa et al., 1988; Nachbar et al., 2018a; Nachbar et al., 2018b; Nachbar et al., 2019; Salzmann et al., 2004b; Tonauer et al., 2023). Irreversible sintering effects with associated reductions of surface area may contribute towards the heat releases (Gärtner et al., 2017; Handa et al., 1988). It has been shown that there is an approximately linear relationship between the heat release during the phase transition and the Φ_c of the starting ice I*sd* material (Carr et al., 2014). The phase transition of ice I*sd* to ice I*h* is certainly complex with a wide distribution of intermediate stages. The kinetics of the phase transition are not well studied and will depend on the details of the stacking disorder of the starting material, the heating rate, the duration of isothermal holds and if re-condensation of subliming H_2O is permitted. The different desorption rates of ice I*sd* and ice I*h* reflecting their different vapour pressures have recently been observed using a quartz crystal microbalance (Rosu-Finsen et al., 2022).

Interestingly, ice I*c*, which can be assumed to be more metastable than ice I*sd*, has been reported to transform to ice I*h* at slightly higher temperatures than ice I*sd* (del Rosso et al., 2020; Komatsu et al., 2020). This has been attributed to the absence of hexagonal stacking in ice I*c* which may act as a catalyst for the conversion of ice I*sd* to ice I*h*.

In the following, we discuss the various environments in the Solar System where a presence of ice I*sd* is possible.

3. Atmospheres of the inner planets

Clouds composed of water ice particles are known to form throughout our Solar System (Mangan et al., 2021; Simon-Miller et al., 2000) and beyond (Faherty et al., 2014). Detailed insights into the properties of these clouds are essential to our understanding of planetary atmospheres. For example, ice particle growth and subsequent precipitation redistributes water, dehydrating rising air masses. Through growth and precipitation mechanisms, ice clouds serve as cold traps, dehydrating air entering the stratosphere on Earth (Peter et al., 2006) and are key to determining how much water is lost to space on Mars (Fedorova et al., 2020). Ice clouds can also exert a substantial influence on the temperature of an atmosphere, interacting with both incoming shortwave radiation and outgoing infrared radiation. In fact, thin ice clouds are thought to have a net warming effect and it has been suggested that high-altitude clouds on early Mars may have warmed the surface sufficiently so that liquid water would have existed (Kite et al., 2021). The roles ice clouds play in planetary atmospheres is strongly affected by the details of the microphysics of clouds. For example, the size and shape of crystals strongly influence their fall speed with implications for cloud lifetime, radiative properties and redistribution of atmospheric constituents. The phase of ice affects all of these cloud microphysical properties and hence, identification of the correct ice phases present in clouds is important for understanding the role of clouds in planetary atmospheres.

In this section, we go on to identify cold cloud types in the atmospheres of Earth, Mars and Venus that occur in a temperature range where the metastable ice I*sd* can form.

3.1. Clouds in the atmosphere of Earth

There are three regions of Earth's atmosphere where cloud formation occurs in the temperature range where ice I*sd* is possible (see Fig. 2(c)). The coldest place on Earth is the summertime polar upper mesosphere where temperatures can regularly be below the ice frost point of ~150 K, and sometimes fall below 100 K, leading to cloud formation at altitudes between ~80 and 90 km (Lübken et al., 2009). These clouds are known as polar mesospheric clouds (PMCs) or noctilucent clouds when observed by eye from Earth's surface in the summer twilight. Ice particles in these clouds also interact with ions and free electrons in the region of the mesopause, which is in the lower ionosphere, and can lead to radar signals called polar summer mesospheric echoes (Rapp and Lubken, 2004). Multiple nucleation mechanisms might be possible in these clouds with nucleation of meteoric smoke likely, but under extreme conditions homogeneous nucleation of amorphous ice is also thought to be feasible (Murray and Jensen, 2010). These clouds redistribute water and in doing so, alter the odd-hydrogen and oxygen chemistry of the polar mesosphere (Murray and Plane, 2005a), as well as providing a surface onto which meteoric metal species are removed, altered and redistributed (Mangan et al., 2017; Murray and Plane, 2005b). There are no direct measurements that can distinguish between ice I*h*, I*sd* or I*c* in these clouds, but they have been shown to be composed predominantly of crystalline ice assumed to be ice I*c* at the time based on the temperature of these clouds (Hervig and Gordley, 2010), although the transient presence of nanoscale amorphous ice particles cannot be readily ruled out. Laboratory work shows that ice deposited at temperatures relevant for the upper mesosphere of Earth can indeed be ice I*sd* (Mangan et al., 2021; Murray et al., 2015a).

Another location in the Earth's atmosphere where ice I*sd* may form is in the northern and southern polar stratosphere, where ice particles can form below ~188 K. The occurrence and nature of polar stratospheric clouds strongly influences ozone chemistry through providing surfaces on which chlorine and bromine species are produced that then go on to catalyse ozone destruction. They also denitrify the atmosphere as nitrate-rich particles grow and sediment, leading to even greater ozone loss. There are several types of polar stratospheric clouds, with clouds containing ice occurring below ~188 K (Lowe and MacKenzie, 2008). Such low temperatures are encountered when air is forced upwards over mountain ranges (Carslaw et al., 1998). Under these conditions aqueous solution droplets predominantly composed of water and nitric acid freeze. Experiments have shown that the ice within frozen aqueous nitric acid droplets is ice I*sd* at temperatures in polar stratospheric clouds (Murray et al., 2005), but the subsequent phase of ice to deposit as the ice particle grow is unknown.

The coldest part of the Earth's troposphere is in the tropics where strong convective activity drives temperatures down to ~180–200 K in the tropical tropopause layer at altitudes of 12 to 18 km (Jensen et al., 2013). As mentioned above, cirrus clouds that form in this region play an important role as cold traps, dehydrating air entering the stratosphere (Peter et al., 2006). Ice crystals in these clouds are thought to form both through heterogeneous nucleation on solid aerosols and through homogeneous freezing of solution droplets containing a mixture of sulphuric acid, ammonium ions and organic species. These tropical cirrus clouds exist in a temperature range where ice I*sd* has been observed in laboratory experiments and observations of very cold cirrus clouds sometimes reveal crystals with trigonal habits that are consistent with ice I*sd* (Heymsfield, 1986; Murray et al., 2015b). Also, the ice that forms from solution droplets that freeze under conditions relevant to the upper troposphere do so to ice I*sd* (Murray et al., 2005). It has been suggested that the transition from a cloud containing metastable crystalline ice to stable ice I*h* would result in a shift to larger ice particles which would sediment more rapidly and lead to dehydration (Murphy, 2003).

3.2. Clouds in the atmosphere of Mars

Water ice clouds form throughout much of the atmosphere of Mars at altitudes up to ~90 km (Fedorova et al., 2020; Määttänen and Montmessin, 2021). The temperature in the Martian atmosphere can fall below 120 K in the mesosphere (Colaprete et al., 1999; Fedorova et al., 2020). The average surface temperature is around 220 K (Montmessin and Määttänen, 2018), but at the poles and in the mesosphere the temperature can fall below 130 K (Piqueux et al., 2016). Hence, many clouds in the Martian atmosphere exist at temperatures where ice I*sd* has been found in the laboratory. Clouds on Mars have broadly been categorised according to their location, with the aphelion cloud belt around the equator and polar hood clouds in both the north and south stretching from the pole to about 45°. Cloud particles in the lower atmosphere likely form on dust grains from the Martian surface, but those in the mesosphere may also form on meteoric smoke particles (Hartwick et al., 2019). Fig. 3(a) shows Martian clouds captured by the Curiosity rover.

3.3. Clouds in the atmosphere of Venus

Far less research has been carried out on Venusian ice clouds, but there are suggestions in the literature that water ice clouds exist, albeit without corroborating observations (Murray et al., 2023; Turco et al., 1983). Satellite measurements reveal that the temperature can fall to below 100 K between 115 and 130 km (Mahieux et al., 2015; Murray et al., 2023). In this region, the atmosphere becomes strongly supersaturated with respect to crystalline ice below around 120–130 K (Murray et al., 2023). Mangan et al. (2021) demonstrated that vapour deposition resulted in ice I*sd* at 125 K and above, but in amorphous ice at lower temperatures. Hence, it is possible that these mesospheric water ice clouds on Venus might consist of some combination of amorphous ice and ice I*sd*. The analysis of the satellite temperature data reveals that these clouds have the potential to form around the globe and at any latitude. However, the observation of these clouds will be challenging due to the expected nanometre scale of the particles.

As well as proposing clouds at around 120 km, Turco et al. (1983) also proposed that ice clouds might form at around 85 km. This region of the atmosphere is at the upper edge of Venus's sulphuric acid cloud layer. Since the atmosphere is supersaturated with respect to crystalline ice at temperatures below about 160 K, it is possible that the sulphuric acid droplets become sufficiently swollen so that they freeze homogeneously in a manner analogous to cirrus formation on Earth (Koop et al., 2000). The resulting 'cirrus' clouds would have properties comparable to those in the Earth's tropical tropopause region, albeit forming at conditions >20 K colder than their terrestrial counterparts. It has been shown that sulphate-solution droplets freeze to ice I*sd* at temperatures below around 200 K (Murray et al., 2005), hence it is likely that any ice that results from these freezing droplets will be ice I*sd*. However, the phase of ice that then deposits on top of the frozen droplets is unclear.

3.4. Relevance of ice Isd in clouds

We now turn to the question of why the phase (ice I*sd*, Ice I*h* or ice I*c*) matters in clouds. As discussed in Sections 1 and 2, the different materials have distinct crystal structures with different thermodynamic properties. Being a metastable form of ice, ice I*sd* has a greater chemical potential than the stable ice I*h* and this means that the vapour pressure over an ice I*sd* crystal is greater than that over an ice I*h* crystal (Nachbar et al., 2019; Shilling et al., 2006) as mentioned previously. This has been suggested to result in a mass-transfer process where ice I*h* crystals would grow at the expense of ice I*sd* crystals, potentially resulting in clouds of fewer but larger ice crystals (Murphy, 2003). In addition, when theoretically describing nucleation using classical nucleation theory, as is commonly done, it is important to include the physical quantities, such

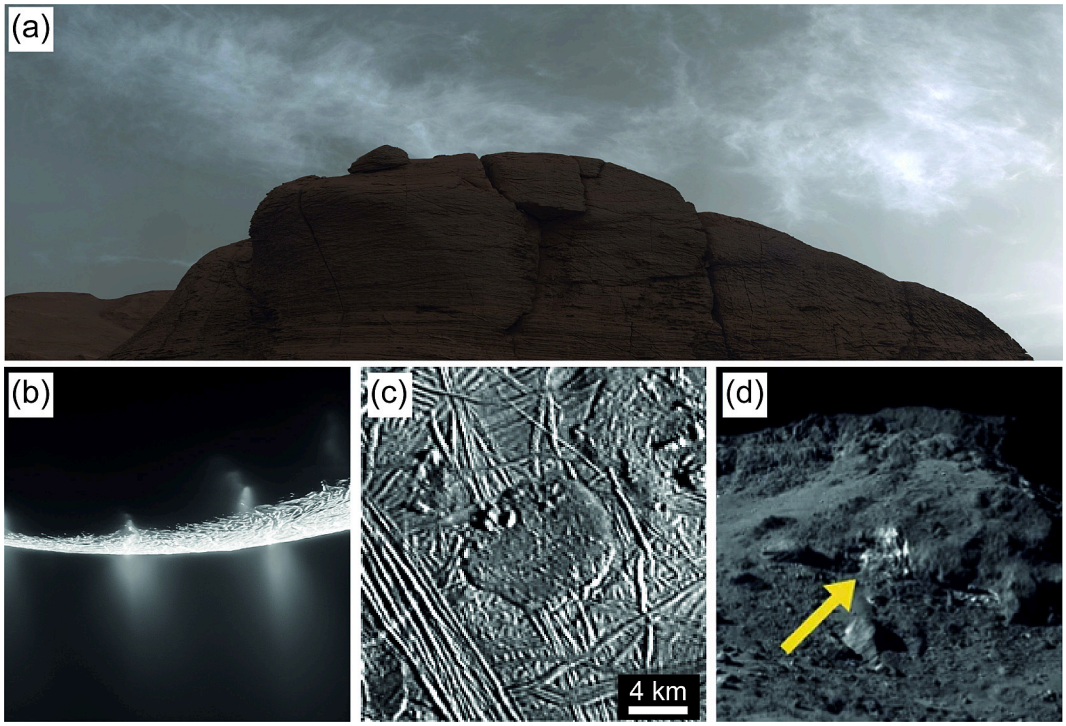

Fig. 3. Potential occurrences of ice I*sd* in the Solar System. (a) False-colour image mosaic of clouds on Mars captured by the Curiosity rover. In the foreground is Mont Mercou, a sedimentary outcrop studied by the rover. Credit: NASA/JPL-Caltech/MSSS. (b) Plumes of vapour and ice at Enceladus imaged by the Cassini spacecraft. Credit: NASA/JPL-Caltech/Space Science Institute. (c) A 'dome'; a quasi-circular feature in Europa's Conamara region with potential cryovolcanic origin, as imaged by the Galileo spacecraft. Note how the dome appears to superpose other features, suggesting effusive flow of a viscous 'cryolava'. Reproduced from Fagents et al. (2003) with permission. (d) A high-albedo patch on comet 67P/Churyumov-Gerasimenko, captured by the Rosetta spacecraft. This patch was interpreted as exposed water ice. Reproduced from Filacchione et al. (2016) with permission.

as vapour pressure, chemical potential and interfacial energy, that correspond to the phase that nucleates.

It is also important to consider the shape, or habit, of ice crystals composed of the different phases of ice. One would expect ice I*c* to form isotropic habits (cubes, octahedra or cuboctahedra), whereas ice I*sd* is expected to form plates or columns with trigonal symmetry (Murray et al., 2015b), as shown in Fig. 4. Interpretation of halo or phase function data can be used to infer the shapes of crystals and perhaps phase. In a study of what type of ice crystals might cause 22° halo displays on Mars, Lemmon et al. (2022) suggested the presence of hexagonal columns of >11 μm length. The 22° halo is caused by refraction through two prism faces of randomly orientated columns that have an angle of 60° between them. The 60° requirement can be satisfied in crystals with either ice I*sd* or ice I*h*. While the observed 22° halo is certainly consistent with the presence of hexagonal columns composed of ice I*h*, it is also consistent with trigonal or scalene columns of ice I*sd*, but inconsistent with ice I*c* habits.

It seems very likely that cold ice clouds will be discovered around other planets and moons in our Solar System and beyond. These clouds have the potential to modify atmospheric chemistry and even play a first-order role in a planet's climate, hence the possible phases of ice should be correctly discussed and considered.

4. Icy moons in the outer Solar System

Beyond the snow-line, the giant planets host a diverse range of icy moons; planetary-scale objects where water ice is a major surface component (Grundy et al., 1999). Icy moons are found at Jupiter (Europa, Ganymede and Callisto; (Pilcher et al., 1972)), Saturn (Enceladus, Titan, Mimas, Phoebe, Dione, Iapetus and others; (Cruikshank, 1980; Fink et al., 1976)), Neptune (Triton; (Cruikshank et al., 2000)) and Uranus (Miranda, Oberon, Titania, Umbriel and others; (Cruikshank, 1980)). Several icy moons, including Europa, Enceladus and Titan, are now prime candidates in the search for life beyond Earth, due to the presence of oceans of liquid water underneath their icy surfaces (Hendrix et al., 2019). The outermost ice-rich layers of icy moons, which have long been assumed to comprise just a single phase of ice (ice I*h*), host a range of active processes with the potential to generate ice I*sd*. This means that the structural diversity of ice on their surfaces could be much greater than previously assumed. In the following, we discuss potential mechanisms for the formation of ice I*sd* in the context of the icy moons of the Solar System.

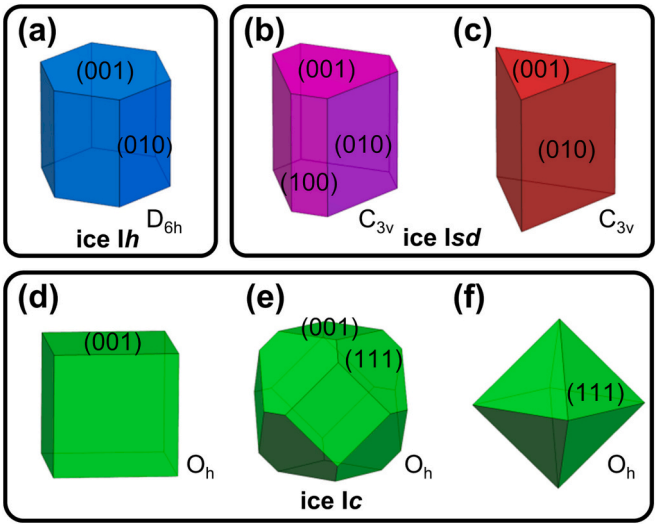

Fig. 4. Possible crystal shapes of single crystals of (a) ice I*h*, (b,c) ice I*sd* and (d–f) ice Ic. The Miller indices (*hkl*) of some of the faces and the crystallographic point groups are indicated. The shapes in (a–c) can have varying axial ratios, forming needles or plates.

4.1. Ice Isd from cryovolcanism

A number of icy moons exhibit geologic evidence for the rapid delivery of water and volatiles onto their surfaces; a process often termed 'cryovolcanism'. A spectacular example of cryovolcanism is found at Saturn's moon Enceladus, where plumes of vapour and ice, very likely sourced directly from Enceladus's subsurface ocean (Postberg et al., 2009), are observed extending up to 9600 km from the surface (Villanueva et al., 2023) (see Fig. 3(b)). There is also evidence for plumes at other icy worlds such as Jupiter's moon Europa (Jia et al., 2018; Sparks et al., 2017) and Ceres, a dwarf planet in the asteroid belt that is similar in size to several of the icy moons (Ruesch et al., 2018).

Multiple routes may exist to producing ice I*sd* in the Enceladus plumes. Vapour deposition must occur within the icy vents that feed the plumes (Schmidt et al., 2008), indicated by the presence of solid grains of near-pure H_2O observed by the Cassini spacecraft (Postberg et al., 2009; Postberg et al., 2011). Temperatures within the vents likely range from near water's triple point at ~273 K to ~200 K ± 20 K at the vent openings on Enceladus's surface (the 'tiger stripes') (Goguen et al., 2013; Schmidt et al., 2008), thus it is unclear whether the pure H_2O grains are grown at low enough temperatures to form ice I*sd*. Ice I*sd* is likely to form where plume vapour is deposited on the surface near the tiger stripes (Newman et al., 2008), where temperatures quickly decrease from ~200 K at the vents to <100 K in the surrounding terrain (Spencer et al., 2006). Indeed, Cassini near-infrared spectra indicate the presence of amorphous ice, which is best explained by vapour deposition at low temperatures.

Ice I*sd* could also form within micrometre-sized aerosolised liquid droplets, which are precursors of the salty ice grains detected by Cassini (Postberg et al., 2009). These droplets contain moderate levels of solutes, including sodium chloride and carbonate (~2 wt%) (Postberg et al., 2009), and likely freeze to ice I*sd* if freezing takes place below ~190 K (Murray and Bertram, 2008; Murray et al., 2005), conditions which are possible in the plumes. Experimental work has also shown that micro-scale confinement of high-salinity phases can occur during rapid freezing of solutions relevant to Enceladus's ocean composition (Fox-Powell and Cousins, 2021). Ice I*sd* could form within these inclusions (Kajiwara et al., 2008), provided that crystallisation is not inhibited entirely by rapid cooling rates or high viscosities.

Multiple icy moons also host surface features indicative of effusive cryovolcanism, where liquids or slushes are extruded onto the surface, including Europa (Bradák et al., 2023; Fagents, 2003; Kattenhorn and Prockter, 2014; Lesage et al., 2021) (see Fig. 3(c)) and Saturn's moon Titan (Lopes et al., 2013). In such systems, where fluids are introduced onto surface temperatures of <100 K, modelling suggests that rapidly-frozen crusts should develop (Quick et al., 2017). Ice I*sd* could form in these crusts, even if the cooling rates in the bulk of the extruded material beneath may be slow enough to allow ice I*h* to form.

4.2. Ice Isd from salt solutions

Stacking disorder could be further promoted by the presence of solutes. Salts have been detected at many icy moons, including on the surface of Europa (Brown and Hand, 2013; King et al., 2022; Ligier et al., 2016; Trumbo et al., 2019), Enceladus (Postberg et al., 2009) and Ganymede (Tosi et al., 2023), meaning there is good reason to expect salt ions to participate in the formation of icy materials within their ice shells. Freezing of salty liquids in the subsurface of icy moons may occur over thousands of years (Chivers et al., 2023), and under these circumstances, ice I*sd* is less likely, as gradual freezing allows interaction between ice and residual liquid, which should lead to relaxation to ice I*h* regardless of initial ice phase or the presence of solutes. However, if cryovolcanic eruptions occur during re-freezing of shallow melt reservoirs (as expected at Europa; (Chivers et al., 2023; Lesage et al., 2020;

Schmidt et al., 2011)), fluids with salt concentrations up to their eutectics could be emplaced into <100 K surface environments. Upon crystallisation at these temperatures they should form ice I*sd* alongside salt phases. Freezing of salty solutions can also lead to fluid confinement due to the development of freeze-concentrated micro-porous inclusions (Buffo et al., 2021; Fox-Powell and Cousins, 2021). Ice I*sd* may crystallise within these inclusions even if the bulk ice is ice I*h* (Kajiwara et al., 2008), leading to the potential for ice I*sd* in cryovolcanically extruded slushes. It must be noted that the extent and efficiency of ice I*sd* formation in the presence of solutes appears composition-dependent (Murray et al., 2005), and should be studied further in the context of cryovolcanic fluids.

4.3. Ice Isd from clathrate hydrates and high-pressure phases of ice

Warming of icy moon ice shells could produce I*sd* from a range of parent materials including gas clathrate hydrates, amorphous ice and high-pressure ices. Warming would also decrease the Φ_c of existing ice I*sd* (see Fig. 2(c)), leaving a potential signature of thermal processing, provided that the ice I*sd* does not convert fully to ice I*h*. Localised heating of ice shell materials could occur at many active icy moons, driven by ascension of buoyant warm ice (diapirism; (Singer et al., 2021)), intrusion of liquid or slush along structural weaknesses (diking; (Manga and Michaut, 2017)), tectonic shear stress (Han and Showman, 2008) or impacts.

Clathrate hydrates are anticipated to be present and stable within the ice shells and sub-ocean high-pressure ice layers of icy moons such as Titan and Europa (Choukroun and Sotin, 2012; Loveday et al., 2001; Mousis et al., 2015) and potentially Enceladus (Bouquet et al., 2015; Kieffer et al., 2006). If these clathrate hydrates dissociate, ice I*sd* would be produced in potentially large quantities. The upper part of Titan's ice shell is likely to be rich in methane clathrate hydrates (Čadek et al., 2021; Choukroun and Sotin, 2012), which dissociate when reaching the surface and near subsurface (Atreya et al., 2006), resulting in the potential for extensive formation of ice I*sd* in Titan's ice shell. Dissociation of clathrate hydrates may also occur through isothermal depressurisation during cryovolcanic eruptions (Kieffer et al., 2006).

The conditions within the deep interiors of some of the larger icy moons, including Titan, Ganymede and Callisto, are compatible with the presence of sub-ocean high-pressure ice phases. On Ganymede, these layers are likely to be composed of ices III, V or VI depending on the depth (Vance et al., 2014) and on Titan of ices II, V or VI (Fortes, 2012). If these ice phases can be incorporated into the overlying ice I shell, and thus recovered at lower pressures, heating may result in the formation of ice I*sd*. However, we consider that this is an unlikely route for ice I*sd* formation, as geophysical modelling suggests that high-pressure ice layers and the ice I outer shell are separated by global liquid oceans (Vance et al., 2014; Vance et al., 2018). Impact events on surface ice may lead to the formation of high-pressure phases of ice which may transform to ice I*sd* as the build-up of pressure subsides.

4.4. Ice Isd from exogenic radiation

Finally, some icy moons, including Europa, can experience bombardment with very highly charged particles (Johnson et al., 2004). Radiation of this sort can induce defects in ice, which has been hypothesised to result in the formation of amorphous ice (Hansen and McCord, 2004). It is also possible that exogenic radiation bombardment of ice I*h* could lead to the formation of stacking faults in ice, or to the alteration of Φ_c of existing ice I*sd*. If so, ice I*sd* could have hemispheric or global distributions at icy worlds, such as Europa. Laboratory experiments are required to understand the potential for radiation to produce ice I*sd* through this pathway, and the extent to which it may affect the structure of existing ice I*sd*.

4.5. Relevance of ice Isd for future investigations of the icy moons

Understanding the potential for the existence of ice I*sd* at the Solar System's icy moons is important for several reasons. For instance, the exothermic conversion of ice I*sd* to ice I*h* may lead to ice shell heat transfer that could not be predicted if only considering ice I*h*. Furthermore, understanding the presence of ice I*sd* could change our interpretation of existing spacecraft data. For example, the formation of ice I*sd* in the Enceladus plumes could play a role in determining plume-gas mixing ratios observed by Cassini. Deposition of vapour on the vent walls is considered to be a major factor influencing the observed ratios of plume gases (Fifer et al., 2022; Glein et al., 2015). Current estimates, which consider only ice I*h*, predict that the net effect of deposition of water vapour is to enrich non-water volatiles in the plumes relative to their oceanic abundances (Fifer et al., 2022). However, if ice I*sd* dominates the vapour-deposition process, the higher saturation vapour pressure of ice I*sd* relative to ice I*h* could mean less water vapour is lost to condensation than currently assumed.

Investigating the distribution and structure of ice I*sd* at icy moons holds great promise for advancing our understanding of these still enigmatic planetary bodies. Future missions will directly search for recently active cryovolcanic regions on Europa, or other icy ocean worlds, as they are vitally important for studying ocean chemistry. As ice I*sd* may be readily produced by cryovolcanic eruptions, its presence may reveal locations where subsurface fluids have recently interacted with the surface environment. Furthermore, as ice I*sd* can convert over time to the more thermodynamically stable ice I*h*, the Φ_c of the material could in principle be employed to estimate its initial formation age, and thus the length of time it has been exposed to degradation in the space environment. However, in practice this will not be possible until the kinetics of ice I*sd* to ice I*h* phase transition under conditions relevant to icy world surfaces have been investigated in the laboratory.

Understanding the thermal history of cryovolcanic ice will also be important, as it may affect preservation of the chemical signature of parent liquid reservoirs. In principle, ice I*sd* offers a means of probing thermal history, as it has been demonstrated that the stacking probabilities relate directly to the ice formation route, as shown in Fig. 2(b). Specific stacking probabilities may also reveal areas of clathrate dissociation, radiative processing or amorphous ice crystallisation, although subsequent thermal processing and radiation may act to overprint signatures of endogenic processes. Comprehensive experimental mapping of first and second-order stacking probabilities across the phase spaces of cooling rates, pressure and ion concentration, as well as an understanding of how heating or irradiation may impact Φ_c, will be needed to fully unlock this potentially rich geological archive encoded into ice I*sd* at icy moons.

5. The far reaches of the Solar System

The Kuiper belt lies beyond the orbit of Neptune and contains large numbers of objects including several dwarf planets such as Pluto, Eris, Haumea, Makemake and Quaoar. The Kuiper belt objects (KBOs) represent the outer part of the protoplanetary disc that did not take part in the formation of planets. Water ice is typically a major constituent of KBOs and centaurs which are KBOs that have moved closer towards the sun (Brown, 2000; Brown et al., 1999; Brown et al., 1998; Merlin et al., 2007; Trujillo et al., 2007). The occurrence of water ice on the surfaces of KBOs can be described with three different categories (Brown et al., 2012): (1) Haumea-type KBOs have surfaces of nearly pure water ice and are thought to represent surface fragments of larger differentiated icy objects (Brown et al., 2007). (2) The largest KBOs can retain gases in their atmospheres leading to frost on their surfaces including water ice. (3) The surfaces of the majority of KBOs are thought to contain complex undifferentiated mixtures including water ice alongside other chemical species.

The surface temperatures of KBOs are typically below 50 K (Jewitt

and Luu, 2004). At these temperatures, amorphous ice is the expected state. Yet crystalline ice has been detected on several KBOs (Brown, 2000; Jewitt and Luu, 2004; Merlin et al., 2007; Trujillo et al., 2007). The origin of the crystalline ice is unclear but must be due to resurfacing events while the levels of radiation appear insufficient to achieve amorphization of the ice (Loeffler et al., 2020). On Pluto, cryovolcanism has been observed (Cruikshank et al., 2019; Singer et al., 2022).

The spectrum of the surface of Haumea was best fitted with a 1:1 mixture of amorphous and (what was noted as) crystalline ice (Pinilla-Alonso et al., 2009). Given the apparent competition between amorphous and crystalline ice, and the generally low temperatures on KBOs, it seems likely that ice I*sd* is the crystalline component and not ice I*h*, which requires much higher temperatures to form than typical at the surface of these objects (see Fig. 2(c)). Following flybys of Pluto and the Arrokoth KBO, the New Horizon probe will continue to explore the Kuiper belt until 2028 (Spencer et al., 2020).

Comets are icy objects originating from the Kuiper Belt and beyond (Mumma and Charnley, 2011). They often display highly eccentric elliptical orbits, which means that flybys relatively close to the Sun are possible. Whipple coined the idea of 'dirty snowballs' (Whipple, 1976), which was later extended to 'icy dirtballs' during NASA's Deep Impact mission where a projectile was fired at the comet Temple 1 (A'Hearn et al., 2005). More recently, ESA succeeded in landing on the 67P/Churyumov-Gerasimenko comet and observed bright albedo patches of water ice on its surface as shown in Fig. 3(d) (Filacchione et al., 2016). The temperature of the surface ice was in the 160–180 K temperature range at the time of the mission which is consistent with the existence of ice I*sd*. In addition to the formation of ice I*sd* on comets through warming of amorphous ice, the vapour deposition route may also be possible as comets undergo complicated diurnal weather cycles (De Sanctis et al., 2015).

Regarding small ice particles at the outskirts of the Solar System and in proto-planetary environments, it is interesting to note that the crystallographic space group of ice I*sd*, *P*3*m*1, (Murray et al., 2015b) allows polar structures which are forbidden by the space groups of ice I*h* and I*c*. Such polarization effects of ice I*sd* could facilitate long-range electrostatic interactions between ice particles which could be an important mechanism for ice accretion processes.

6. Conclusions

There is every reason to assume that ice I*sd* exists in diverse environments in the Solar System and potentially in large quantities. Ice I*c* on the other hand requires quite special starting materials for its formation and was only recently created in laboratories. Ice I*c* is therefore probably much less abundant than ice I*sd* unless other, as yet unknown, production routes are possible. There is certainly now a need to critically assess previous discussions of 'ice I*c*' in the scientific literature to decide if 'ice I*sd*' would have been a more accurate description of the materials under investigation.

Contrary to ices I*h* and I*c*, ice I*sd* is a structurally highly complex material that encompasses a wide range of possible structures with different Φ_cs and memory effects within its stacking sequences. This structural complexity means that ice I*sd* samples can potentially contain information about their route of formation and thermal histories. This provides an exciting opportunity to use ice I*sd* as a marker material for atmospheric and geological processes in the Solar System.

Despite recent advances exploring the fundamental properties of ice I*sd* there is still much that is not understood about this complex material. For example, the details of the kinetics of the ice I*sd* to ice I*h* transition with its wide range of intermediate states need to be explored in greater detail in particular with the aim to predict the extent of the conversion over astronomic and geological time scales. The influences of the presence of additional chemical species such as salts on the details of the stacking characteristics of ice I*sd* is also still poorly understood as are the effects of confinement and surface-templating during the growth from the vapour phase.

Regarding the characterisation and detection of ice I*sd*, diffraction, and powder X-ray diffraction in particular, has so far given the most detailed insights. X-ray diffraction has been used onboard the Mars Curiosity rover to reveal the mineralogy of dust samples in the Gale crater (Bish et al., 2013). These techniques could perhaps be applied to samples from the surface of icy worlds. The X-ray diffraction pattern of ice I*sd* ($\Phi_c = 0.5$) in Fig. S2 was calculated using the experimental parameters and noise characteristics of the Chemistry and Mineralogy (CheMin) X-ray diffraction instrument onboard Curiosity (Blake et al., 2012). The diffuse scattering due to the stacking disorder of ice I*sd* is clearly visible in the 26–31° range which means that it should be possible to detect ice I*sd* with the CheMin instrument. The signal-to-noise ratio of the diffuse scattering component with a maximum around 28° is about 12:1.

Further studies should also focus on exploring the potential benefits of using electron diffraction (Huang et al., 2023), which may be well suited for the remote detection of ice I*sd*. The spectroscopic signatures of stacking disorder in spectroscopy also deserve further attention including in particular infrared spectroscopy which is widely used in observational astronomy. Raman spectroscopy, which has been successfully deployed on Mars by NASA's Perseverance rover and has been considered for future icy world missions (*e.g.*, Sharma et al., 2020) also holds promise as a tool for identifying ice I*sd* and probing its cubicity (Carr et al., 2014). But also, it should be noted that ice I*sd* has so far not been detected on Earth despite good reasons to assume that it exists in our atmosphere. In this sense, efforts to identify ice I*sd* on Earth could be the first stepping stone for developing the remote technology needed for wider searches in the Solar System. Proving that ice I*sd* exists outside the lab will certainly be a next exciting milestone in our efforts to understand the role and importance of water ice across the Solar System.

Declaration of Competing Interest

The authors declare that they have no known competing financial interests or personal relationships that could have appeared to influence the work reported in this paper.

Data availability

No data was used for the research described in the article.

Appendix A. Supplementary data

Additional calculated neutron and X-ray diffraction data of ice I*sd*. Supplementary data to this article can be found online at https://doi.org/10.1016/j.icarus.2023.115897.

References

A'Hearn, M.F., et al., 2005. Deep impact: excavating comet Tempel 1. Science. 310, 258–264.
Amaya, A.J., et al., 2017. How cubic can ice be? J. Chem. Phys. Lett. 8, 3216–3222.
Arnold, G.P., Finch, E.D., Rabideau, S.W., Wenzel, R.G., 1968. Neutron-diffraction study of ice polymorphs. III. Ice Ic. J. Chem. Phys. 49, 4365–4369.
Atreya, S.K., et al., 2006. Titan's methane cycle. Planet. Space Sci. 54, 1177–1187.
Baker, J.M., Dore, J.C., Behrens, P., 1997. Nucleation of ice in confined geometry. J. Phys. Chem. B 101, 6226–6229.
Bertie, J.E., Calvert, L.D., Whalley, E., 1963. Transformations of ice II, ice III, and ice V at atmospheric pressure. J. Chem. Phys. 38, 840–846.
Bertie, J.E., Calvert, L.D., Whalley, E., 1964. Transformations of ice VI and ice VII at atmospheric pressure. Can. J. Chem. 42, 1373–1378.
Bish, D.L., et al., 2013. X-ray diffraction results from Mars Science Laboratory: mineralogy of rocknest at Gale Crater. Science. 341, 1238932.
Blake, D., et al., 2012. Characterization and calibration of the CheMin mineralogical instrument on Mars Science Laboratory. Space Sci. Rev. 170, 341–399.
Bouquet, A., Mousis, O., Waite, J.H., Picaud, S., 2015. Possible evidence for a methane source in Enceladus' ocean. Geophys. Res. Lett. 42, 1334–1339.
Bradák, B., Kereszturi, Á., Gomez, C., 2023. Tectonic analysis of a newly identified putative cryovolcanic field on Europa. Adv. Space Res. 72, 4064–4073.

Brown, M.E., 2000. Evidence for crystalline water and ammonia ices on Pluto's satellite Charon. Science. 287, 107–109.
Brown, M.E., Hand, K.P., 2013. Salts and radiation products on the surface of Europa. Astron. J. 145, 110–117.
Brown, R.H., Cruikshank, D.P., Pendleton, Y., Veeder, G.J., 1998. Identification of water ice on the centaur 1997 CU26. Science. 280, 1430–1432.
Brown, R.H., Cruikshank, D.P., Pendleton, Y., 1999. Water ice on Kuiper Belt object 1996 TO66. Astrophys. J. 519, L101.
Brown, M.E., Barkume, K.M., Ragozzine, D., Schaller, E.L., 2007. A collisional family of icy objects in the Kuiper belt. Nature. 446, 294–296.
Brown, M.E., Schaller, E.L., Fraser, W.C., 2012. Water ice in the Kuiper Belt. Astron. J. 143, 146.
Buffo, J.J., Meyer, C.R., Parkinson, J.R.G., 2021. Dynamics of a solidifying icy satellite shell. J. Geophys. Res. Planets. 126, e2020JE006741.
Burton, E.F., Oliver, W.F., 1935. X-ray diffraction patterns of ice. Nature. 135, 505–506.
Čadek, O., Kalousová, K., Kvorka, J., Sotin, C., 2021. The density structure of Titan's outer ice shell. Icarus. 364, 114466.
Carr, T.H.G., Shephard, J.J., Salzmann, C.G., 2014. Spectroscopic signature of stacking disorder in ice I. J. Phys. Chem. Lett. 5, 2469–2473.
Carslaw, K.S., et al., 1998. Increased stratospheric ozone depletion due to mountain-induced atmospheric waves. Nature. 391, 675–678.
Celli, M., Ulivi, L., del Rosso, L., 2020. Raman investigation of the ice Ic–ice I*h* transformation. J. Phys. Chem. C 124, 17135–17140.
Chivers, C.J., Buffo, J.J., Schmidt, B.E., 2023. Stable brine layers beneath Europa's chaos. Planet. Sci. 4, 159.
Choukroun, M., Sotin, C., 2012. Is Titan's shape caused by its meteorology and carbon cycle? Geophys. Res. Lett. 39, L04201.
Colaprete, A., Toon, O.B., Magalhães, J.A., 1999. Cloud formation under Mars Pathfinder conditions. J. Geophys. Res. Planets. 104, 9043–9053.
Cruikshank, D.P., 1980. Near-infrared studies of the satellites of Saturn and Uranus. Icarus. 41, 246–258.
Cruikshank, D.P., et al., 2000. Water ice on Triton. Icarus. 147, 309–316.
Cruikshank, D.P., et al., 2019. Recent cryovolcanism in Virgil Fossae on Pluto. Icarus. 330, 155–168.
De Sanctis, M.C., et al., 2015. The diurnal cycle of water ice on comet 67P/Churyumov-Gerasimenko. Nature. 525, 500–503.
del Rosso, L., et al., 2020. Cubic ice Ic without stacking defects obtained from ice XVII. Nat. Mat. 19, 663–668.
Deutsch, A.N., Neumann, G.A., Head, J.W., 2017. New evidence for surface water ice in small-scale cold traps and in three large craters at the north polar region of Mercury from the Mercury Laser Altimeter. Geophys. Res. Lett. 44, 9233–9241.
Dowell, L.G., Rinfret, A.P., 1960. Low-temperature forms of ice as studied by X-ray diffraction. Nature. 188, 1144–1148.
Dowell, L.G., Moline, S.W., Rinfret, A.P., 1962. A low-temperature X-ray diffraction study of ice structures formed in aqueous gelatin gels. Biochim. Biophys. Acta 59, 158–167.
Elarby-Aouizerat, A., Jal, J.F., Dupuy, J., Schildberg, H., Chieux, P., 1987. Comments on the ice Ic structure and Ic to I*h* phase transformation mechanism: a neutron scattering investigation of ice precipitates in glassy $LiCl.D_2O$. J. Phys. Colloques. 48. C1-465-C1-470.
Fagents, S.A., 2003. Considerations for effusive cryovolcanism on Europa: The post-Galileo perspective. J. Geophys. Res. Planets 108, 5139.
Faherty, J.K., Tinney, C.G., Skemer, A., Monson, A.J., 2014. Indications of water clouds in the coldest known Brown Dwarf. Astrophys. J. Lett. 793, L16.
Falenty, A., Kuhs, W.F., 2009. "Self-preservation" of CO_2 gas hydrates—surface microstructure and ice perfection. J. Phys. Chem. B 113, 15975–15988.
Fedorova, A.A., et al., 2020. Stormy water on Mars: the distribution and saturation of atmospheric water during the dusty season. Science. 367, 297–300.
Fifer, L.M., Catling, D.C., Toner, J.D., 2022. Chemical fractionation modeling of plumes indicates a gas-rich, moderately alkaline Enceladus Ocean. Planet. Sci. J. 3, 191.
Filacchione, G., et al., 2016. Exposed water ice on the nucleus of comet 67P/Churyumov–Gerasimenko. Nature. 529, 368–372.
Fink, U., Larson, H.P., Gautier III, T.N., Treffers, R.R., 1976. Infrared spectra of the satellites of Saturn: identification of water ice on Iapetus, Rhea, Dione, and Tethys. Astrophys. J. 207, L63–L67.
Fortes, A.D., 2012. Titan's internal structure and the evolutionary consequences. Planet. Space Sci. 60, 10–17.
Fox-Powell, M.G., Cousins, C.R., 2021. Partitioning of crystalline and amorphous phases during freezing of simulated Enceladus Ocean fluids. J. Geophys. Res. Planets 126 e2020JE006628.
Gärtner, S., et al., 2017. Micrometer-sized water ice particles for planetary science experiments: influence of surface structure on collisional properties. Astrophys. J. 848, 96.
Glein, C.R., Baross, J.A., Waite, J.H., 2015. The pH of Enceladus' ocean. Geochim. Cosmochim. Acta 162, 202–219.
Goguen, J.D., et al., 2013. The temperature and width of an active fissure on Enceladus measured with Cassini VIMS during the 14 April 2012 South Pole flyover. Icarus. 226, 1128–1137.
Grundy, W.M., Buie, M.W., Stansberry, J.A., Spencer, J.R., Schmitt, B., 1999. Near-infrared spectra of icy outer solar system surfaces: remote determination of H_2O ice temperatures. Icarus. 142, 536–549.
Halukeerthi, S.O., Shephard, J.J., Talewar, S.K., Evans, J.S.O., Rosu-Finsen, A., Salzmann, C.G., 2020. Amorphous mixtures of ice and C_{60} fullerene. J. Phys. Chem. A 124, 5015–5022.
Han, L., Showman, A.P., 2008. Implications of shear heating and fracture zones for ridge formation on Europa. Geophys. Res. Lett. 35. L03202.
Handa, Y.P., Klug, D.D., Whalley, E., 1986. Difference in energy between cubic and hexagonal ice. J. Chem. Phys. 84, 7009–7010.
Handa, Y.P., Klug, D.D., Whalley, E., 1988. Energies of the phases of ice at low temperature and pressure relative to ice I*h*. Can. J. Chem. 66, 919–924.
Hansen, G.B., McCord, T.B., 2004. Amorphous and crystalline ice on the Galilean satellites: A balance between thermal and radiolytic processes. J. Geophys. Res. Planets 109, E01012.
Hansen, T.C., Koza, M.M., Kuhs, W.F., 2008. Formation and annealing of cubic ice: I. Modelling of stacking faults. J. Phys. Condens. Matter 20, 285104.
Hansen, T.C., Sippel, C., Kuhs, W.F., 2014. Approximations to the full description of stacking disorder in ice I for powder diffraction. Z. Kristallogr. 230, 75–86.
Hart, A.G., Hansen, T.C., Kuhs, W.F., 2018. A Markov theoretic description of stacking-disordered aperiodic crystals including ice and opaline silica. Acta Crystallogr. A 74, 357–372.
Hartwick, V.L., Toon, O.B., Heavens, N.G., 2019. High-altitude water ice cloud formation on Mars controlled by interplanetary dust particles. Nat. Geosci. 12, 516–521.
Hendrix, A.R., et al., 2019. The NASA roadmap to ocean worlds. Astrobiology. 19, 1–27.
Hervig, M.E., Gordley, L.L., 2010. Temperature, shape, and phase of mesospheric ice from solar occultation for ice experiment observations. J. Geophys. Res. Atmos. 115, D15208.
Heymsfield, A.J., 1986. Ice particles observed in a cirriform cloud at −83-degrees-C and implications for polar stratospheric clouds. J. Atmos. Sci. 43, 851–855.
Hobbs, P.V., 1974. Ice Physics. Clarendon Press, Oxford.
Huang, X., et al., 2023. Tracking cubic ice at molecular resolution. Nature. 617, 86–91.
Hussmann, H., Sotin, C., Lunine, J.I., 2015. 10.18 - interiors and evolution of icy satellites. In: Schubert, G. (Ed.), Treatise on Geophysics (Second Edition). Elsevier, Oxford, pp. 605–635.
Jagodzinski, H., 1949. Eindimensionale Fehlordnung in Kristallen und ihr Einfluss auf die Röntgeninterferenzen. I. Berechnung des Fehlordnungsgrades aus den Röntgenintensitäten. Acta Crystallogr. 2, 201–207.
Jensen, E.J., et al., 2013. Ice nucleation and dehydration in the Tropical Tropopause Layer. Proc. Natl. Acad. Sci. 110, 2041–2046.
Jewitt, D.C., Luu, J., 2004. Crystalline water ice on the Kuiper belt object (50000) Quaoar. Nature. 432, 731–733.
Jewitt, D., Chizmadia, L., Grimm, R., Prialnik, D., 2007. Water in the small bodies of the solar system. In: Reipurth, B., Jewitt, D., Keil, K. (Eds.), Protostars and Planets V. University of Arizona Press, pp. 863–878.
Jia, X., Kivelson, M.G., Khurana, K.K., Kurth, W.S., 2018. Evidence of a plume on Europa from Galileo magnetic and plasma wave signatures. Nat. Astron. 2, 459–464.
Johnson, R.E., Carlson, R.W., Cooper, J.F., Paranicas, C., Moore, M.H., Wong, M.C., 2004. In: Bagenal, F., Dowling, T.E., McKinnon, W.B. (Eds.), Cambridge planetary science, 1. Cambridge University Press.
Journaux, B., et al., 2020. Large ocean worlds with high-pressure ices. Space Sci. Rev. 216, 7.
Kajiwara, K., Thanatuksom, P., Murase, N., Franks, F., 2008. Cubic ice can be formed directly in the water phase of vitrified aqueous solutions. Cryo Lett. 29, 29–34.
Kattenhorn, S.A., Prockter, L.M., 2014. Evidence for subduction in the ice shell of Europa. Nat. Geosci 7, 762–767.
Kieffer, S.W., Lu, X., Bethke, C.M., Spencer, J.R., Marshak, S., Navrotsky, A., 2006. A clathrate reservoir hypothesis for Enceladus' south polar plume. Science. 314, 1764–1766.
King, O., Fletcher, L.N., Ligier, N., 2022. Compositional mapping of Europa using MCMC modeling of near-IR VLT/SPHERE and Galileo/NIMS observations. Planet. Sci. J. 3, 72.
Kite, E.S., Steele, L.J., Mischna, M.A., Richardson, M.I., 2021. Warm early Mars surface enabled by high-altitude water ice clouds. Proc. Natl. Acad. Sci. 118, e2101959118.
Kohl, I., Mayer, E., Hallbrucker, A., 2000. The glassy water–cubic ice system: a comparative study by X-ray diffraction and differential scanning calorimetry. Phys. Chem. Chem. Phys. 2, 1579–1586.
Komatsu, K., et al., 2020. Ice Ic without stacking disorder by evacuating hydrogen from hydrogen hydrate. Nat. Commun. 11, 464.
König, H., 1943. Eine kubische Eismodifikation. Z. Kristallogr. 105, 279–286.
Koop, T., Luo, B.P., Tsias, A., Peter, T., 2000. Water activity as the determinant for homogeneous ice nucleation in aqueous solutions. Nature. 406, 611–614.
Kuhs, W.F., Bliss, D.V., Finney, J.L., 1987. High-resolution neutron powder diffraction study of ice I_c. J. Phys. Colloq. C1 (48), 631–636.
Kuhs, W.F., Genov, G., Staykova, D.K., Hansen, T., 2004. Ice perfection and onset of anomalous preservation of gas hydrates. Phys. Chem. Chem. Phys. 6, 4917–4920.
Kuhs, W.F., Sippel, C., Falentya, A., Hansen, T.C., 2012. Extent and relevance of stacking disorder in "ice Ic". Proc. Natl. Acad. Sci. U. S. A. 109, 21259–21264.
Kwok, S., 2007. Physics and Chemistry of the Interstellar Medium. University Science Books, Sausalito, USA.
Lemmon, M.T., et al., 2022. Hexagonal prisms form in water-ice clouds on Mars, producing halo displays seen by perseverance rover. Geophys. Res. Lett. 49 e2022GL099776.
Lesage, E., Massol, H., Schmidt, F., 2020. Cryomagma ascent on Europa. Icarus. 335, 113369.
Lesage, E., Schmidt, F., Andrieu, F., Massol, H., 2021. Constraints on effusive cryovolcanic eruptions on Europa using topography obtained from Galileo images. Icarus. 361, 114373.
Li, S., et al., 2018. Direct evidence of surface exposed water ice in the lunar polar regions. Proc. Natl. Acad. Sci. U. S. A. 115, 8907–8912.
Ligier, N., Poulet, F., Carter, J., Brunetto, R., Gourgeot, F., 2016. VLT/SINFONI observations of Europa: new insights into the surface composition. Astron. J. 151, 163.

Loeffler, M.J., Tribbett, P.D., Cooper, J.F., Sturner, S.J., 2020. A possible explanation for the presence of crystalline H_2O-ice on Kuiper Belt Objects. Icarus. 351, 113943.
Lopes, R.M.C., et al., 2013. Cryovolcanism on titan: new results from Cassini RADAR and VIMS. J. Geophys. Res. Planets. 118, 416–435.
Loveday, J.S., et al., 2001. Stable methane hydrate above 2 GPa and the source of Titan's atmospheric methane. Nature. 410, 661–663.
Lowe, D., MacKenzie, A.R., 2008. Polar stratospheric cloud microphysics and chemistry. J. Atmos. Sol. Terr. Phys. 70, 13–40.
Lübken, F.J., Lautenbach, J., Höffner, J., Rapp, M., Zecha, M., 2009. First continuous temperature measurements within polar mesosphere summer echoes. J. Atmos. Sol. Terr. Phys. 71, 453–463.
Määttänen, A., Montmessin, F., 2021. Clouds in the Martian Atmosphere. Oxford University Press.
Mahieux, A., et al., 2015. Update of the Venus density and temperature profiles at high altitude measured by SOIR on board Venus Express. Planet. Space Sci. 113-114, 309–320.
Malkin, T.L., Murray, B.J., Brukhno, A.V., J. A, Salzmann, C.G., 2012. Structure of ice crystallized from supercooled water. Proc. Natl. Acad. Sci. U. S. A. 109, 1041–1045.
Malkin, T.L., Murray, B.J., Salzmann, C.G., Molinero, V., Pickering, S.J., Whale, T.F., 2015. Stacking disorder in ice I. Phys. Chem. Chem. Phys. 17, 60–76.
Manga, M., Michaut, C., 2017. Formation of lenticulae on Europa by saucer-shaped sills. Icarus. 286, 261–269.
Mangan, T.P., Frankland, V.L., Murray, B.J., Plane, J.M.C., 2017. The fate of meteoric metals in ice particles: effects of sublimation and energetic particle bombardment. J. Atmos. Sol. Terr. Phys. 161, 143–149.
Mangan, T.P., Plane, J.M.C., Murray, B.J., 2021. The phase of water ice which forms in cold clouds in the mesospheres of Mars, Venus, and Earth. J. Geophys. Res. Planets. 126 e2020JE006796.
McMillan, J.A., Los, S.C., 1965. Vitreous ice: irreversible transformations during warm-up. Nature. 206, 806–807.
Merlin, F., Guilbert, A., Dumas, C., Barucci, M.A., de Bergh, C., Vernazza, P., 2007. Properties of the icy surface of the TNO 136108 (2003 EL). A&A. 466, 1185–1188.
Millot, M., et al., 2019. Nanosecond X-ray diffraction of shock-compressed superionic water ice. Nature. 569, 251–255.
Mishima, O., Calvert, L.D., Whalley, E., 1984. 'Melting ice' I at 77 K and 10 kbar: a new method of making amorphous solids. Nature. 310, 393–395.
Montmessin, F., Määttänen, A., 2018. Temperature, clouds, and aerosols in the terrestrial bodies of the solar system. In: Deeg, H.J., Belmonte, J.A. (Eds.), Handbook of Exoplanets. Springer International Publishing, Cham, pp. 1–29.
Mousis, O., et al., 2015. Methane clathrates in the solar system. Astrobiology. 15, 308–326.
Mumma, M.J., Charnley, S.B., 2011. The chemical composition of comets—emerging taxonomies and natal heritage. Annu. Rev. Astron. Astrophys. 49, 471–524.
Murphy, D.M., 2003. Dehydration in cold clouds is enhanced by a transition from cubic to hexagonal ice. Geophys. Res. Lett. 30, 2230,.
Murray, B.J., Bertram, A.K., 2008. Inhibition of solute crystallisation in aqueous H^+–NH_4^+–SO_4^{2-}–H_2O droplets. Phys. Chem. Chem. Phys. 10, 3287–3301.
Murray, B.J., Jensen, E.J., 2010. Homogeneous nucleation of amorphous solid water particles in the upper mesosphere. J. Atmos. Sol. Terr. Phys. 72, 51–61.
Murray, B.J., Plane, J.M.C., 2005a. Modelling the impact of noctilucent cloud formation on atomic oxygen and other minor constituents of the summer mesosphere. Atmos. Chem. Phys. 5, 1027–1038.
Murray, B.J., Plane, J.M.C., 2005b. Uptake of Fe, Na and K atoms on low-temperature ice: implications for metal atom scavenging in the vicinity of polar mesospheric clouds. Phys. Chem. Chem. Phys. 7, 3970–3979.
Murray, B.J., Knopf, D.A., Bertram, A.K., 2005. The formation of cubic ice under conditions relevant to Earth's atmosphere. Nature. 434, 202–205.
Murray, B.J., Malkin, T.L., Salzmann, C.G., 2015a. The crystal structure of ice under mesospheric conditions. J. Atmos. Sol. Terr. Phys. 127, 78–82.
Murray, B.J., Salzmann, C.G., Heymsfield, A.J., Dobbie, S., Neely, R.R., Cox, C.J., 2015b. Trigonal ice crystals in Earth's atmosphere. Bull. Am. Met. Soc. 96, 1519–1531.
Murray, B.J., Mangan, T.P., Määttänen, A., Plane, J.M.C., 2023. Ephemeral Ice Clouds in the Upper Mesosphere of Venus. J. Geophys. Res. Planets 128, e2023JE007974.
Nachbar, M., Duft, D., Leisner, T., 2018a. The vapor pressure over nano-crystalline ice. Atmos. Chem. Phys. 18, 3419–3431.
Nachbar, M., Duft, D., Leisner, T., 2018b. Volatility of amorphous solid water. J. Phys. Chem. B 122, 10044–10050.
Nachbar, M., Duft, D., Leisner, T., 2019. The vapor pressure of liquid and solid water phases at conditions relevant to the atmosphere. J. Chem. Phys. 151, 064504.
Newman, S.F., Buratti, B.J., Brown, R.H., Jaumann, R., Bauer, J., Momary, T., 2008. Photometric and spectral analysis of the distribution of crystalline and amorphous ices on Enceladus as seen by Cassini. Icarus 193, 397–406.
Palacios, O.D.C., Inaba, A., Andersson, O., 2010. Low-temperature heat capacity of a two-dimensionally ordered structure of ice crystallized from glycerol aqueous solutions. Thermochim. Acta 500, 106–110.
Peter, T., Marcolli, C., Spichtinger, P., Corti, T., Baker, M.B., Koop, T., 2006. When dry air is too humid. Science 314, 1399–1402.
Petrenko, V.F., Whitworth, R.W., 1999. Physics of Ice. Oxford University Press, Oxford.
Pilcher, C.B., Ridgway, S.T., McCord, T.B., 1972. Galilean satellites: identification of water frost. Science. 178, 1087–1089.
Pinilla-Alonso, N., Brunetto, R., Licandro, J., Gil-Hutton, R., Roush, T.L., Strazzulla, G., 2009. The surface of (136108) Haumea (2003 EL61), the largest carbon-depleted object in the trans-Neptunian belt. A&A. 496, 547–556.
Piqueux, S., et al., 2016. Discovery of a widespread low-latitude diurnal CO_2 frost cycle on Mars. J. Geophys. Res. Planets. 121, 1174–1189.
Playford, H.Y., Whale, T.F., Murray, B.J., Tucker, M.G., Salzmann, C.G., 2018. Analysis of stacking disorder in ice I using pair distribution functions. J. Appl. Crystal. 51, 1211–1220.
Postberg, F., et al., 2009. Sodium salts in E-ring ice grains from an ocean below the surface of Enceladus. Nature. 459, 1098–1101.
Postberg, F., Schmidt, J., Hillier, J., Kempf, S., Srama, R., 2011. A salt-water reservoir as the source of a compositionally stratified plume on Enceladus. Nature. 474, 620–622.
Prakapenka, V.B., Holtgrewe, N., Lobanov, S.S., Goncharov, A.F., 2021. Structure and properties of two superionic ice phases. Nat. Phys. 17, 1233–1238.
Quick, L.C., Glaze, L.S., Baloga, S.M., 2017. Cryovolcanic emplacement of domes on Europa. Icarus. 284, 477–488.
Rapp, M., Lubken, F.J., 2004. Polar mesosphere summer echoes (PMSE): review of observations and current understanding. Atmos. Chem. Phys. 4, 2601–2633.
Rosu-Finsen, A., Chikani, B., Salzmann, C.G., 2022. Thermal desorption of H_2O ice: from nanoscale films to the bulk. Mon. Notices Royal Astron. Soc. 517, 1919–1927.
Rosu-Finsen, A., et al., 2023. Medium-density amorphous ice. Science. 379, 474–478.
Ruesch, O., et al., 2018. Bright carbonate surfaces on Ceres as remnants of salt-rich water fountains. Icarus. 320, 39–48.
Salzmann, C.G., 2019. Advances in the experimental exploration of water's phase diagram. J. Chem. Phys. 150, 060901.
Salzmann, C.G., Murray, B.J., 2020. Ice goes fully cubic. Nat. Mat. 19, 586–587.
Salzmann, C.G., Mayer, E., Hallbrucker, A., 2004a. Effect of heating rate and pressure on the crystallization kinetics of high-density amorphous ice on isobaric heating between 0.2 and 1.9 GPa. Phys. Chem. Chem. Phys. 6, 5156–5165.
Salzmann, C.G., Mayer, E., Hallbrucker, A., 2004b. Thermal properties of metastable ices IV and XII: comparison, isotope effects and relative stabilities. Phys. Chem. Chem. Phys. 6, 1269–1276.
Salzmann, C.G., Murray, B.J., Shephard, J.J., 2015. Extent of stacking disorder in diamond. Diamond Relat. Mater. 59, 69–72.
Schmidt, J., Brilliantov, N., Spahn, F., Kempf, S., 2008. Slow dust in Enceladus' plume from condensation and wall collisions in tiger stripe fractures. Nature. 451, 685–688.
Schmidt, B.E., Blankenship, D.D., Patterson, G.W., Schenk, P.M., 2011. Active formation of 'chaos terrain' over shallow subsurface water on Europa. Nature. 479, 502–505.
Sharma, S.K., Porter, J.N., Misra, A.K., Acosta-Maeda, T.E., Angel, S.M., McKay, C.P., 2020. Standoff Raman spectroscopy for future Europa Lander missions. J. Raman Spectosc. 51, 1782–1793.
Shephard, J.J., Klotz, S., Vickers, M., Salzmann, C.G., 2016. A new structural relaxation pathway of low-density amorphous ice. J. Chem. Phys. 144, 204502.
Shilling, J.E., Tolbert, M.A., Toon, O.B., Jensen, E.J., Murray, B.J., Bertram, A.K., 2006. Measurements of the vapor pressure of cubic ice and their implications for atmospheric ice clouds. Geophys. Res. Lett. 33, L17801.
Simon-Miller, A.A., Conrath, B., Gierasch, P.J., Beebe, R.F., 2000. A detection of water ice on Jupiter with voyager IRIS. Icarus. 145, 454–461.
Singer, K.N., McKinnon, W.B., Schenk, P.M., 2021. Pits, uplifts and small chaos features on Europa: morphologic and morphometric evidence for intrusive upwelling and lower limits to ice shell thickness. Icarus. 364, 114465.
Singer, K.N., et al., 2022. Large-scale cryovolcanic resurfacing on Pluto. Nat. Commun. 13, 1542.
Sparks, W.B., et al., 2017. Active cryovolcanism on Europa? Astrophys. J. Lett. 839, L18.
Spencer, J.R., et al., 2006. Cassini encounters Enceladus: background and the discovery of a south polar hot spot. Science. 311, 1401–1405.
Spencer, J.R., et al., 2020. The geology and geophysics of Kuiper Belt object (486958) Arrokoth. Science. 367, eaay3999.
Takeya, S., et al., 2005. Particle size effect of CH_4 hydrate for self-preservation. Chem. Eng. Sci. 60, 1383–1387.
Talewar, S.K., et al., 2019. Gaseous "nanoprobes" for detecting gas-trapping environments in macroscopic films of vapor-deposited amorphous ice. J. Chem. Phys. 151, 134505.
Tonauer, C.M., Yamashita, K., Rosso, L.d., Celli, M., Loerting, T., 2023. Enthalpy change from pure cubic ice Ic to hexagonal ice Ih. J. Phys. Chem. Lett. 14, 5055–5060.
Tosi, F., et al., 2023. Salts and organics on Ganymede's surface observed by the JIRAM spectrometer onboard Juno. Nat. Astron. https://doi.org/10.1038/s41550-023-02107-5.
Trujillo, C.A., Brown, M.E., Barkume, K.M., Schaller, E.L., Rabinowitz, D.L., 2007. The surface of 2003 EL61 in the near-infrared. Astrophys. J. 655, 1172.
Trumbo, S.K., Brown, M.E., Hand, K.P., 2019. Sodium chloride on the surface of Europa. Sci. Adv. 5, eaaw7123.
Tschauner, O., et al., 2018. Ice-VII inclusions in diamonds: evidence for aqueous fluid in Earth's deep mantle. Science. 359, 1136–1139.
Turco, R.P., Toon, O.B., Whitten, R.C., Keesee, R.G., 1983. Venus: mesospheric hazes of ice, dust, and acid aerosols. Icarus. 53, 18–25.
Vance, S., Bouffard, M., Choukroun, M., Sotin, C., 2014. Ganymede's internal structure including thermodynamics of magnesium sulfate oceans in contact with ice. Planet. Space Sci. 96, 62–70.
Vance, S.D., et al., 2018. Geophysical investigations of habitability in ice-covered ocean worlds. J. Geophys. Res. Planets. 123, 180–205.
Vigier, G., Thollet, G., Vassoille, R., 1987. Cubic and hexagonal ice formation in water-glycerol mixture (50% w/w). J. Cryst. Growth 84, 309–315.
Villanueva, G.L., et al., 2023. JWST molecular mapping and characterization of Enceladus' water plume feeding its torus. Nat. Astron. 7, 1056–1062.
Whipple, F.L., 1976. Background of modern comet theory. Nature. 263, 15–19.